2019

Development and Sensory Experience Dependent Regulation of Microglia in Barrel Cortex

Joshua C. Brumberg
CUNY Queens College

John Kalambogias
CUNY Graduate Center

Chia-Chien Chen
CUNY Graduate Center

Safraz Khan
CUNY Queens College

Titus Son
CUNY Queens College

See next page for additional authors

Development and Sensory Experience Dependent Regulation of Microglia in Barrel Cortex

John Kalambogias[1], Chia-Chien Chen[2, 5], Safraz Khan[3], Titus Son[4], Racheli Wercberger[4], Carolyn Headlam[5], Cindy Lin[5], Joshua C. Brumberg[1,2,4,5*]

1. Neuroscience Doctoral Subprogram (Biology), The Graduate Center, City University of New York, New York, New York 10016
2. Neuropsychology Doctoral Subprogram (Psychology), The Graduate Center, City University of New York, New York, New York 10016
3. Biology Department, Queens College, City University of New York, Flushing, New York 11367
4. Neuroscience Major, Queens College, City University of New York, Flushing, New York 11367
5. Psychology Department, Queens College, City University of New York, Flushing, New York 11367

Words in Abstract: 199
Total Pages: 39
Figures: 8
Tables: 2
Supplemental Tables: 4
Running Title: Microglia in Barrel Cortex

***Corresponding Author:**
Joshua C. Brumberg, PhD,
Department of Psychology
Queens College, CUNY
65-30 Kissena Boulevard
Flushing, NY 11367, USA
Telephone Number: 718-997-3541
Fax Number: (718) 997-3257
E-mail: joshua.brumberg@qc.cuny.edu

Abstract

The barrel cortex is within the primary somatosensory cortex of the rodent, and processes signals from the vibrissae. Much focus has been devoted to the function of neurons, more recently, the role of glial cells in the processing of sensory input has gained increasing interest. Microglia are the principal immune cells of the nervous system that survey and regulate the cellular constituents of the dynamic nervous system. We investigated the normal and disrupted development of microglia in barrel cortex by chronically depriving sensory signals via whisker trimming for the animals' first postnatal month. Using immunohistochemistry to label microglia, we performed morphological reconstructions as well as densitometry analyses as a function of developmental age and sensory experience. Findings suggest that both developmental age and sensory experience has profound impact on microglia morphology. Following chronic sensory deprivation, microglia undergo a morphological transition from a monitoring or resting state to an altered morphological state, by exhibiting expanded cell body size and retracted processes. Sensory restoration via whisker regrowth returns these morphological alterations back to age-matched control values. Our results indicate that microglia may be recruited to participate in the modulation of neuronal structural remodeling during developmental critical periods and in response to alteration in sensory input.

Key Words

barrel cortex; microglial morphology; sensory deprivation; somatosensory cortex; vibrissae

RRID: AB_2224402

RRID: AB_2339427

RRID: AB_2336126

RRID: AB_2313661

RRID: AB_2339392

RRID: AB_2340111

Introduction

The central nervous system (CNS) of mammals is composed of many different types of cells, which include both neuronal and glial cells (Parkhurst & Gan, 2010). Neurons underlie sensory processing, cognitive functioning, motor execution and planning, among other tasks. Glial cells on the other hand, are at least as numerous as neurons, and are traditionally thought to play supportive roles, such as maintaining homeostasis within the brain (Azevedo et al., 2009). Microglial cells are a class of glia that mature over the first few weeks of life (Arnoux et al., 2013; Hoshiko, Arnoux, Avignone, Yamamoto, & Audinat, 2012), and comprise the brain's immune system, constantly scouring the nervous system in search of abnormalities and attempt to remove necrotic/damaged tissue (Hanisch & Kettenmann, 2007). Once microglia develop and differentiate, they transition morphologically from amoeboid to a ramified form, entering a "surveillance" state (Graeber & Streit, 2010). Under non-pathological conditions, microglia constantly extend and retract their processes, monitoring the extracellular environment in the CNS (Nimmerjahn, Kirchhoff, & Helmchen, 2005).

Microglial activation was once believed to be an all or nothing event (Kettenmann, Hanisch, Noda, & Verkhratsky, 2011). However, recent studies have shown that microglia cells adapt to environmental conditions and activation is reversible and context dependent. During the surveillance states microglial cells make temporary contacts with astrocytes, neuronal axon terminals, and dendritic spines, in a sense "feeling out" the local environment (Tremblay, Lowery, & Majewska, 2010). During pathological conditions, microglia change their functional state and become activated. The activated state results in the thickening and retraction of microglia processes, and migrating towards the site of injury where they multiply in numbers and

perform the appropriate responses. For example, microglia may phagocytose cellular debris. They may also present antigens, or secrete proteases that may degrade extracellular matrix or myelin, and promote further microglial motility (Mosser, Baptista, Arnoux, & Audinat, 2017; Tremblay et al., 2010). Within the cerebral cortex, synaptic stripping mediated by microglia has been reported, in which active microglial processes physically separate presynaptic axon terminals from postsynaptic dendritic spines (Z. Chen et al., 2014; Trapp et al., 2007; Tremblay et al., 2010). Additionally, microglia may facilitate synaptic pruning where synaptic elements are eliminated by phagocytosis (Paolicelli et al., 2011; Stephan, Barres, & Stevens, 2012; Whitelaw, 2018). Microglia, therefore, play a critical role in synaptic remodeling (Arcuri, Mecca, Bianchi, Giambanco, & Donato, 2017a; Miyamoto et al., 2016; Wu, Dissing-Olesen, MacVicar, & Stevens, 2015). They also respond to alterations in sensory input (Arcuri et al., 2017a; Eyo & Wu, 2013; Michell-Robinson et al., 2015; Tremblay et al., 2010) and early disruption of microglia can dramatically impact neural development (Arnoux, Hoshiko, Sanz Diez, & Audinat, 2014; Hanamsagar et al., 2018; Miyamoto et al., 2016; Stevens et al., 2007; Ueno et al., 2013).

Previous studies have investigated the role of microglial cells in the primary visual and auditory cortices (Nimmerjahn et al., 2005; Tremblay et al., 2010; Tremblay & Majewska, 2011). However, the normal development of microglia and the effect of sensory deprivation on microglia in the somatosensory cortex, specifically the barrel cortex, have not been studied. The barrel cortex is the brain region of rodents which processes somatosensory information from the vibrissae (whiskers) of the mystacial pad, and has been widely used as a model for studying cellular development within neocortical circuits (Feldman & Brecht, 2005; Petersen, 2007). Each barrel is an aggregate of neurons in layer IV that represent the whiskers on the contralateral side of the mystacial pad in topographic fashion. Whisker-related neocortical information processing

is highly specialized and sensitive (Carvell & Simons, 1990). Previously we have shown that chronically trimming the rodent's whiskers for the first postnatal month has been shown to have profound impacts on the neuronal morphology of the barrel cortex (C.-C. Chen, Tam, & Brumberg, 2012), decreasing the amount of extracellular matrix (McRae, Rocco, Kelly, Brumberg, & Matthews, 2007), and increasing levels of the enzyme tissue plasminogen activator (C.-C. Chen, Chu, & Brumberg, 2015), which has been implicated in matrix reductions. Ultimately, sensory deprivation leads to changes in barrel responses to sensory input, thereby disrupting whisking related behavior (Carvell & Simons, 1996). Although it has been shown that microglial processes play a pivotal role in the remodeling of dendritic spines in the visual system (Miyamoto et al., 2016; Tremblay & Majewska, 2011), their roles in the somatosensory barrel system has yet to be fully elucidated (Hoshiko et al., 2012). The present study aims to quantitatively characterize the morphological profile of microglia in the barrel cortex of mice across development and to explore the impact of sensory deprivation.

Materials and Methods

Animals and Experimental Groups

All procedures were conducted in accordance with the Queens College CUNY Institutional Animal Care and use Committee (protocol No. 100) and National Institutes of Health guidelines concerning the responsible use of animals in research. CD-1 mice of either sex (Charles River Laboratories, Wilmington, MA) were used for the experiments. Mice were housed in standard plastic cages with woodchip bedding with unlimited access to food and water and exposed to 12-hour light/dark cycles. Pregnant moms were monitored to ensure proper postnatal age, and mice were sacrificed at different developmental ages (Postnatal day (P) 2: n=6 animals, P14: n= 9 animals, P30: n= 7 animals, P45: n= 8 animals, P60: n= 6 animals). These time points were chosen to parallel our earlier neuronal studies (C.-C. Chen, Bajnath, & Brumberg, 2015; C.-C. Chen et al., 2012). To investigate the impact of sensory deprivation, littermates were randomly assigned into either the control group (n=7) or the sensory deprived group (n=7). Whiskers were trimmed (for details see below) unilaterally every other day for the first postnatal month starting on P0 (day of birth). To determine the role of sensory restoration, a different group (n=4) of mice had their whiskers unilaterally trimmed on alternate days from P0 to P30, and the whiskers were allowed to regrow, permitting sensory input from P31 to P60 (“regrow” animals). These animals were compared to a group of age matched (P60) control littermates (n=4). Table 1 details the total number of animals in each experimental group. Developmental ages were picked based on previous studies in the laboratory allowing for direct comparisons (C.-C. Chen, Bajnath, et al., 2015; C.-C. Chen, Chu, et al., 2015; C.-C. Chen et al., 2012; McRae et al., 2007).

Whisker trimming

Sensory deprivation was achieved by unilaterally trimming all the whiskers every other day starting from birth. Trimming of just one mystacial pad was utilized due to the unilateral input to the barrel cortex (Erzurumlu & Gaspar, 2012). All whiskers were clipped to the base of the follicle on the right side of the mystacial pad using microsurgical scissors. Starting from P14, all animals were briefly anesthetized with isoflurane (Aerrane) for 1 to 3 minutes during trimming to prevent the animals from excessive movement. Control animals were handled and anesthetized similarly, except their whiskers were not trimmed (C.-C. Chen, Chu, et al., 2015; C.-C. Chen et al., 2012; McRae et al., 2007). The right ears of the animals within the regrow group were hole-punched to differentiate them from their age-matched control littermates.

Immunohistochemistry

Mice were anesthetized with an intraperitoneal injection of Euthasol (Virbac AH, Inc.) and transcardially perfused first with 0.9% NaCl in dH_20 followed by ice cold (4^oC) 4% paraformaldehyde in 0.01M phosphate buffer (PB) at selected postnatal days and then the brains were post-fixed in 4% paraformaldehyde in 0.01M PB for seven days. The fixed tissue was coronally sectioned at 70 μm in 0.01M phosphate buffered saline (PBS) on a vibratome (Vibratome 3000) using the slowest cutting speed and the highest amplitude to avoid cutting artifact. The right hemisphere of each brain was marked with a slight cut (outside of barrel cortex) in order to differentiate the left and the right hemisphere. Brain slices were then washed with 0.01M PBS, quenched for endogenous peroxidase activity for 20 mins with 1% H_2O_2 and 0.5% methanol in 0.1M PBS, and then permeabilized with 0.7% Triton X-100 and blocked with

5% normal rabbit serum at room temperature for 1 hour (h). Primary antibodies specific to microglia (Abcam, Cat# ab 5075, host goat, ionized calcium binding adaptor protein (Iba-1), 1:1000, RRID: AB_2224402 (Villa et al., 2007) were administered to floating brain sections for approximately three days at 4ºC. Although Iba-1 largely labels microglia, it can also label some lymphocytes, but most Iba-1+ cells are presumed to be microglia (Ahmed et al., 2007). Following primary antibody incubation, slices were washed for 30 min in PBS, and treated with biotinylated anti-goat secondary (Vector Labs or Jackson Immuno, host rabbit, 1:500 dilution, RRID: AB_2339427, RRID: AB_2336126) for 2.5 h. Slices were washed for another 30 min in PBS, then incubated in avidin-biotin HRP (horse radish peroxidase) complex (ABC solution, Vector Labs) for 1 hour, washed in PBS for 30 min again, and then incubated in 3,3'-Diaminobenzidine (DAB) + H_2O_2 for 5 minutes. Sections were then extensively washed in 0.01M PBS, counterstained with Hoechst solution (Sigma-Aldrich, dilution 1:10000, final solution 0.12 μg/ml), dehydrated in ascending concentration of ethanol series, defatted in a xylene substitute (Safeclear II, ThermoFisher Scientific), and mounted using paramount mounting medium (Sigma-Aldrich) and sealed with clear nail-polish. For each round of the immunohistochemistry procedure, we also included a brain slice without any primary antibodies to ensure the labeling is not due to non-specific binding.

In some cases, the surface markers of microglia were assessed using fluorescent labeling techniques. Animals were treated as described above and then following sectioning the brain slices were processed for dual immunocytochemistry. Brain slices were initially washed with 0.01M PBS (3 washes for 10 minutes each), and then permeabilized and blocked with a cocktail of 0.5% Triton X-100 and 5% Normal Rabbit Serum in which they incubated for 1 hour at room temperature. Primary antibodies specific to microglia (Iba-1, 1:1000 dilution, Abcam), and to

MHC-II a cell surface marker expressed by some microglia (Kigerl et al., 2009) (Dako, now a part of Agilent, Cat# M0775, host mouse, anti-MHC-II, 1:100, RRID: AB_2313661) were administered to floating brain slices and left to incubate at 4ºC for three days. Following primary antibody incubation, slices were washed again in 0.01M PBS (3 washes for 10 minutes each) and treated with a cocktail of anti-goat and anti-mouse secondary antibodies, conjugated to rhodamine red-X and FITC, respectively (Jackson Immuno, Cat# 305-025-045; 315-095-045, 1:250 dilution, RRID: AB_2339392; RRID: AB_2340111) for 2-2.5 hours in the dark. Slices were washed in 0.01M PBS, and incubated in Hoescht solution (Sigma-Aldrich, 1:10000 dilution, final solution 0.12µg/ml) for 30-40 minutes in the dark. Slices were then washed again, mounted onto slides using Vectashield (Vector Labs), and sealed with clear nail polish.

Confocal Imaging and Quantifying

For the immunofluorescence studies, we imaged the microglia with a confocal microscope, the FV10i (UPLSAP60X oil immersion lens, Olympus, NA =1.35). Hoechst labeled cells were excited by a light source with a wavelength of 405 nm and an emission wavelength of 455 nm. For imaging FITC and rhodamine labeled cells, we used a light source with excitation wavelengths at 473 nm and 551 nm, and an emission wavelength of 519 nm and 591 nm, respectively, filter sets are native to the FV10i. Laser power was manually set for each image stack to maximize signal while minimizing saturation. Brain sections were mapped on to the screen; the barrel cortex was identified while under lens magnification of 10x, which was then increased to a magnification of 60x for image stack acquisition (confocal aperture = 2.5µm). All stacks were taken with the x-y dimensions of 212.13µm x 212.13µm (512x512 pixels), and

between 20 to 40 *z*-steps, at 0.747μm/step. For each *z*-step, an average of eight scans were taken and averaged together to optimize image stack quality.

Cells were then counted from each image stack using the computer-assisted program Neurolucida (MBF Bioscience, Inc.). Different markers were used to mark off Hoescht+, Iba-1+, and MHC-II+ cells, and exported to NeuroExplorer (MBF Biosciences, Inc.) software where quantitative analyses were performed. Cell density was calculated (number of immunoreactive cells in a stack / volume of the stack) for each cell type, and graphs were compiled using the software SigmaPlot.

Optical Density Measurements of Iba-1 Expression

Optical density (absorbance) of Iba-1+ cell expression were quantified in a nonbiased fashion to assay for microglia expression using the computer assisted program Neurolucida (MBF Bioscience, Inc). Measurements were performed on an Olympus BX51 microscope equipped with a high-resolution digital camera (Optronics Microfire), with a motorized stage (Ludl, Thornwood, NY), and an x-y-z axis encoder connected to a Windows Pentium 4 PC (Paxinos & Franklin, 2001) and a Hg 100W light source with appropriate fluorescent filters. Optical density measurements were conducted using the 10x lens (Plan N, 10x, Numerical Aperture (NA) = 0.10). Contour maps were manually generated for layers 2/3, 4, 5, 6 and the cortical white matter (see Figure 3A). Images of Hoechst labeled cortical barrels were identified by observing the characteristic cluster of cells that are typically found within layer IV and by matching with an atlas of the mouse brain (Paxinos & Franklin, 2001). The Neurolucida function "collect luminescence" was used to measure the brightness of the contour maps for each layer and white matter (Figure 3A). The brightness of the white matter was first assessed and adjusted

to 200 ± 3 (on a scale of 0-255, 0 being the darkest) under the observation that very little microglia labeling are observed in white matter (comparisons of the optical density of the white matter across animals and conditions did not vary, although variation has been seen using other immunohistochemical markers (Hart, Wyttenbach, Perry, & Teeling, 2012). Brightness of each cortical layer was then obtained, and normalized to the brightness of the white matter of that specific animal (Optical density = [brightness of cortical layer]/[brightness of white matter]). The brightness/contrast, RGB ratio, optical gain, gamma, image integration time and aperture size were held constant across all conditions (experimental and control) and all images were taken during the same microscope session. Optical density measures of Iba-1 immunoreactivity from the deprived cortex (contralateral to trimming) were taken for all animals in the sensory deprivation study at P30 (n=7 animals) and compared to the measurements taken from the cortex ipsilateral to the trimming from the same animals. Animals in the regrow groups were not measured. Optical density measurements of Iba-1 immunohistological expression are assumed to reflect the overall expression of microglia rather than just their density since both cell bodies and processes impact the intensity of staining (C.-C. Chen, Chu, et al., 2015).

Quantification of Microglia within the Barrel Cortex

To further validate the results from the optical density experiments, we performed stereological quantification of microglial population density within the barrel cortex. We quantified the number of Iba-1+ cells in the P30 control as well as P30 sensory deprived groups in all cortical layers. We used the software Stereo Investigator (MBF Bioscience Ver. 10.0) to estimate the actual number of microglia within each layer as we have done previously (Barrera et al., 2013). We used the optical fractionator method to perform systematic sampling of

populations distributed within a series of serial sections to estimate the population number in a volume, yielding unbiased estimates of population number. Histological processes often result in shrinkage along the Z-axis of a section due to greater exposed surface area, which may cause inconsistent section thickness. To account for this we obtained the average section thickness of our sections (see below) to determine the thickness of counting frames and the guard zones for each counted section. In order to accomplish this we averaged the thickness of ten random sections (measured to be approximately 40 μm) and this thickness was used to determine the guard zone (14 μm (7 μm on the top and bottom of the slice)).

Similar to previous studies from the lab (Barrera et al., 2013), to initiate the optical fractionator we used a low magnification lens (4x) to draw a contour map within the barrel cortex that defined laminar borders. A high magnification lens (60x oil emersion, NA=1.4) was used for subsequent counting, the size of the counting frame was set at 250 x 250 μm, which is large enough to contain, on average, six cells in a given focal plane. For each lamina, 20 random sites were quantified. During each counting procedure, we manually focused the objective to accurately determine the top and bottom of each section. A cell was counted: (i) if it lies completely inside the counting frame; (ii) if it crosses a green (inclusion) line but not a red (exclusion) line. The grid spacing as well as counting frame size set at the beginning of the experiment was constant throughout the study. Once counting for the region of interest was completed, all data were exported into excel file for further analyses. In order to ensure that there is no experimental bias throughout the analyses, a blinded experimenter analyzed all the data collected from the stereology experiment.

Morphological Reconstruction of Microglial Cells

Individual microglia cells from layer IV of barrel cortex were imaged using Neurolucida (100x, NA = 1.40, oil immersion) by varying the depth of the z-plane to ensure optimal clarity for accurate and precise morphological reconstructions. Layer IV barrels were determined from the Hoechst staining which clearly indicated the labeled cortical barrels [Chroma Technology Corp; excitation 350 nm, emission 460 nm, dichroic 400 nm], as well as by matching with a previously published atlas of the mouse brain (Paxinos & Franklin, 2001). Iba-1 positive cells within layer IV were selected randomly throughout the generated contour map and only cells within the contour map were selected. We selected only cells that appeared to have complete labeling (with no cut processes/soma and possessed distal endings that tapered to a fine point) for our 3D reconstructions. Electron microscopic studies have shown that Iba-1 appears to label complete microglial cells (Shapiro, Perez, Foresti, Arisi, & Ribak, 2009). Microglial cells expressing Iba-1 in layer IV were reconstructed in three dimensions using our microscope which was outfitted with a mechanical stage attached to a computer with Neurolucida (MBF Biosciences Inc.). Reconstructed microglia were then analyzed to obtain morphological information on process length, number of processes, number of process ends, as well as cell body size. Table 1 details the number of cells in each group.

Morphological Analysis of Microglial Cells

The software Neurolucida (MBF Bioscience, Inc.) was used to reconstruct the morphology of the Iba-1+ microglial cell in three-dimensions. Somatic shape and size, process structure and branching patterns were traced and analyzed as previously described[29]. For each reconstructed microglial cell, we measured 1) cell body perimeter, 2) cell body area, 3) aspect ratio = feret max/feret min (feret max = maximum diameter, feret min = minimum diameter

perpendicular to the feret max, as the aspect ratio approaches 1, it is indicative that the soma is closer to a symmetric shape, e.g. circle or square); 4) somatic compactness = [$\sqrt{4/\pi}$) x area]/(feret max); a somatic compactness closer to 1 is indicative of a more compact soma; 5) convexity = (convex contour)/perimeter); 6) somatic form factor = (4π x area)/perimeter^2); this value directly reflects the complexity of the somatic perimeter; a higher value directly represents a more complex somatic perimeter; 7) somatic roundness = (4 x area)/(π x feret max^2); 8) somatic solidity, the ratio of somata area as a whole over convex area; 9) quantity of total processes per branch order. We also analyzed the following metrics from the microglia processes: 10) quantity of total processes nodes; 11) quantity of total processes ends; 12) number of total processes length; 13) total processes mean length; 14) total processes surface area; 15) total processes mean surface area; 16) total processes volume; 17) total processes mean volume; 18) process length; 19) process ends.

Sholl Analysis

Sholl's (Sholl, 1956) method was used to further the morphological characteristics of reconstructed Iba-1+ immunoreactive microglial cells in the software, NeuroExplorer (MBF Bioscience, Inc.). Sholl places concentric circles around the center of the cell's soma to analyze the three dimensional structure of cells. The starting radius was 10 μm with subsequent radius increments of 5 μm. Using concentric sphere analysis, we recorded the number of intersections and the process length passing through the shells of each concentric sphere. Statistical analysis described below.

Statistical Analysis

Iba-1 expression as a function of cortical lamina in the barrel cortex contralateral to the trimming (P30 sensory deprived) was compared to expression levels in the ipsilateral (control) cortex using a paired t-test for all the unilaterally trimmed animals. One way ANOVAs were used to compare all sensory deprived paradigms (P30 sensory deprived animals, P60 regrow) relative to the control animals in layer IV of the barrel cortex of all the morphological components measured. A Mixed-Model ANOVA were used to compare Iba-1 expression as a function of cortical lamina in the barrel cortex across development (P7, P14, P30, P45, P60). If there were for indications of statistical significances, Tukey's HSD (Honestly Significant Difference) test was used post-hoc for comparisons between conditions. One-way ANOVAs were also used to compare the morphological components across development (P2, P14, P30, P45, P60). Tukey HSD test was later used for all pair-wise comparisons following rank-based ANOVA. For the Sholl analysis, a mixed-model ANOVA (condition × distance from soma) was performed for the number of intersections and process length. Subsequently, Scheffé's method was used to adjust significance levels for multiple comparisons. For the analysis of the confocal data a non-parametric text of variance was used (Mann-Whitney U). For comparisons of reconstructed microglia, each cell was considered an independent sample. Statistical tests were run using Sigma Stat (version 3.5 Systat Software Inc.) and Statistica (version 7.1 StatSoft Inc.) on a PC. An alpha level of $p<0.05$ was set *a priori* to determine statistical significance.

Results

Iba-1 Expression Varies Across Development and Laminae

Our Iba-1 immunohistochemistry protocol clearly labeled microglial cell body and processes within the barrel cortex (Figure 1). Microglia under normal healthy conditions exhibited a ramified morphological profile, characterized by a small cell body and processes that elongated and elaborated with age (Figure 1). Iba-1 immunoreactivity patterns at various developmental ages were compared across cortical laminae (Figure 2A, 2B). In normal development, Iba-1 immunoreactivity steadily increased up to P45 in all observed cortical laminae (Mixed-model ANOVA followed by Tukey HSD, $p<0.05$), but not in white matter where microglia are scarce (see Supplementary Table S1-S5 and Figure 2B), in fact the relative luminance of the white matter did not differ across the developmental ages quantified. Between P45 and P60, however, the immunohistological expression of Iba-1 decreased. Furthermore, a composite analysis showed microglia are most prevalent (Tukey HSD, $p<0.05$) in the supragranular layers (layer 2/3) (see Supplementary Table 1, Figure 3B). To confirm the optical density experiment data, we conducted a stereological quantification to obtain the estimated population of microglia within the barrel cortex. The results confirmed our optical density data, that microglia are most prevalent in the supragranular layers ($p<0.05$ compared to all other cortical layers, Figure 6B). In sum, we observed that Iba-1 expression varied as a function of developmental age, peaking around P45; and microglia population are highest in the supragranular layers.

Microglial Morphology

We then quantified the morphological changes of microglia over the first two postnatal months in control animals. Three-dimensional morphological profile of microglial cells were reconstructed and examined at various developmental time points (see Table 1) using Neurolucida (for representative cells see Figure 2). The morphological presentation of microglial cells varied as the animals matured. Over time, the processes length, number of processes ends, and aspect ratio all increased, with both processes ends and aspect ratio peaking at P14 (Figure 4). We observed that the cell body perimeter and area generally decreased across development (Figures 4A,B), while no significant changes in the aspect ratio were observed (Figure 4C), suggesting that the changes in soma size were done uniformly rather than shrinking along a particular axis. There was also no considerable change in the number of processes (Figure 4D), despite a significant change in the process ends ($p<0.04$) as well as in the process length ($p<0.006$) observed across development (Figure 4E-F). The increase in length of the microglial processes peaked at P30 while the number of ends peaked earlier at P14. Although microglia have been shown to exist in many different shapes and sizes (Lawson, Perry, Dri, & Gordon, 1990) the relatively small variances (see error bars in Figure 4) suggest that we have a fairly homogeneous sample. The changes in the number of processes ends and processes length directly reflect the increase in morphological complexity of microglia, suggesting there are significantly more interactions with their environment.

Based on our positive finding of increased complexity of microglial morphology as a function of developmental age, we followed up with a Sholl analysis to further elucidate the extent of morphological complexity of microglial processes. The number of intersections, and process length were analyzed as a function of distance from the cell body (Figure 5A,

Supplementary Table 4). The greatest numbers of processes were observed 10-15 μm from the cell body. P14, P30, P45 and P60 animals had longer processes compared to those from microglia reconstructed from P2 animals. Processes length is at its highest at P30 ($p< 0.05$), then decrease by P60. Overall, the peak number of intersections was approximately 10-15 μm from the cell body. Similar to the process length, we observed a steady increase ($p<0.05$) in the number of endings until P30 animals, followed by a decrement during the second postnatal month.

Sensory Deprivation Impacts Microglial Morphology

Our previous research has shown that sensory experience can dramatically impact neuronal structure and function (C.-C. Chen, Bajnath, et al., 2015; C.-C. Chen et al., 2012). We asked whether this phenomenon could be generalized to the microglial population by investigating how absence of sensory experience during development may impact the microglial structure. We focused on time points we have previously examined in neural tissue (C.-C. Chen, Bajnath, et al., 2015; C.-C. Chen, Chu, et al., 2015; C.-C. Chen et al., 2012). We first compared Iba-1 immunoreactivity between control and sensory-deprived corticies. Laminar boundaries were generated and optical density was measured (as previously mentioned) to compare microglial patterns [P30 deprived barrel cortex {trim (contralateral to trimming)}, P30 nondeprived barrel cortex {control (ipsilateral to trimming)}, n=7 animals]. Despite slightly higher optical densities of Iba-1 immunoreactivity in the deprived barrels in every cortical lamina, no statistically significant differences were observed ($p>0.05$ for all cortical layers, Figure 6A). We further confirmed this finding with stereological methods (Figure 6B) in which we also saw no significant changes of microglial population density ($p>0.05$ for all). The increased cell body size following deprivation (see below) contributed to more occlusion of light

passing through the brain tissue, which accounts for the differences of results between optical density and stereology. However, it is important to note that both methods yielded the same finding, in which the density of microglial population is not affected by sensory deprivation. It is also worth noting that the consistent findings between our stereology and optical density provided important cross-validation of data reliability (Figure 6A, B).

Next, we explored how sensory experience can influence morphological development of microglia. Similarly to previously described, we fully reconstructed labeled microglia and compared in layer IV of P30 nondeprived barrel cortex (control) and P30 sensory deprived barrel cortex (trim) (Figures 7 and 8). We focused on layer IV of the barrel cortex due to its pivotal role as main recipient layer of lemniscal thalamocortical afferents (Feldman & Brecht, 2005; Petersen, 2007). Microscopic observation revealed qualitative differences in microglia morphology following 30 days of trimming, with microglia in sensory deprived cortices having noticeably larger cell bodies and shorter processes (Figure 7A, B). Allowing the whiskers to regrow for a month allowed the microglia to return to their normal morphological phenotype (Figure 7C, D).

Although the overall numbers of microglial processes were not significantly affected by chronic sensory deprivation (Figure 8E), the processes' length were significantly decreased and number of processes' ends unchanged following unilateral whisker trimming ($p's<0.05$, Figure 8F-G). In addition to changes in the processes, cell body area also increased following sensory deprivation ($p<0.008$, Figure 8H, also see Table 2). Our data suggest that the microglia cell bodies were expanding uniformly as opposed to along a specific axis. The significant shortening of microglia processes suggest that sensory deprivation induced a transition of microglia into an altered morphological state.

Next, we asked whether sensory restoration (allowing previously trimmed whiskers to regrow to full length) could revert previously morphologically altered microglia to their normal cellular structures. We found that mice with their sensations restored (P0-30 trim, P31-60 whisker regrow) exhibited similar numbers of microglia processes ($p>0.05$, Figure 8E), length of microglia processes ($p>0.05$, Figure 8F), processes ending points ($p>0.05$, Figure 8G), and microglial cell body size ($p>0.05$, Figure 8H) compared with the P60 age-match control group. The results suggested that following a period of sensory restoration, all of the fine structures of microglia returned to control conditions. Taken together, the observed morphological changes suggested that sensory deprivation activates microglial cells and a period of sensory restoration returns the microglia to their surveillance state.

Microglia surface markers

Change in microglia states have been previously correlated with changes in the expression of different surface antigens (Vinet et al., 2016). Given that sensory deprivation impacted microglia morphology we next sought to see if it impacted the expression of MHC-II a cell surface marker that has been associated with activated microglia (Italiani & Boraschi, 2014; Kigerl et al., 2009). We characterized simultaneously the relative distribution of MHC-II+ and Iba-1+ microglia as a function of one month of sensory deprivation. Microglia were labeled with an antibody to Iba-1 (as above, Figure $9A_2$, B_2), and double-labeled with anti-MHC-II, a surface antigen that is specifically expressed by many activated microglia (Ng & Ling, 1997) (Figure 9 A_3, B_3). Qualitatively, images of the sensory deprived animals resembled their control counterparts (Figure 9A, B). Both the Iba-1 and the MHC-II antibodies were immunoreactive throughout the microglia soma and processes. In order to quantify the effect of sensory

deprivation on the presence of molecular markers that are associated with activated microglia, the total numbers of Iba-1+ cells, as well as MHC-II+ cells, were manually counted from confocal *z*-stacks taken from the layer IV barrels (approximately 3 stacks per animal; $n = 10$ animals in the deprivation group, $n = 4$ animals in the control group). The same was done for Hoechst+ nuclei from the same sections. Negative controls (secondary antibody incubation without primary antibody incubation and primary antibody incubation without secondary antibody incubation) revealed no detectable staining. There was no significant difference between the sensory deprived and control groups with regard to the percentage of Iba-1+ cells expressing MHC-II (Figure 9D). Optical density measures of Iba-1 immunoreactivity from the deprived cortex (contralateral to trimming) were taken for all animals -II in the barrel cortex, there are many other markers of microglial activation (Korzhevskii & Kirik, 2016) that may be impacted by sensory deprivation and warrant further investigation.

Discussion

The current study aims to understand the impact that postnatal development and sensory-experience have on structural morphogenesis of microglia. We find that Iba-1 expression levels increased over the first postnatal month and a half, before returning to adult levels by the end of the second postnatal month. This developmental pattern is observed in all laminae within mouse barrel cortex, with the supragranular layers displaying the highest overall densities of microglia. In addition, we observed alterations in multiple morphological parameters (e.g., soma size, processes ends and length) as the animals matured into adulthood as has been shown previously (Arnoux et al., 2013). Interestingly, following chronic sensory deprivation, the microglial somata increased in size and their processes retracted, consistent with microglial cells transitioning into an altered morphological state, which may have functional ramifications, although the phenotypic distribution did not change. These results indicate that morphological alterations of microglia are associated with changes in the sensory input.

Microglia's Role in Normal Development

Microglia have been shown to play a role in the normal development of cortical circuits (Hanamsagar et al., 2018; Miyamoto et al., 2016; Schafer & Stevens, 2015; Wu et al., 2015). When the microglia chemokine receptor Cx3Cr1 was genetically deleted, synaptic pruning was delayed (Hoshiko et al., 2012; Paolicelli et al., 2011). Previous studies have shown that the largest numbers of newborn microglia appear during the first two postnatal weeks, non-randomly distributed throughout the developing brain 9/16/2019 9:36:00 AM. Microglia cells reside at specific locations such as regions where there are high rates of cell death, proximity to

developing blood vessels, and in close association with radial glial cells (Pont-Lezica et al., 2011). In the mature brain, microglia are also found in greater density in the telencephalon, especially in myelinated regions such as barrel cortex (Czeh, Gressens, & Kaindl, 2011).

Microglia cells are capable of phagocytosis with filopodia acting as phagocytic "tentacles" extending and retracting there processes (Czeh et al., 2011; Kress et al., 2007; Napoli & Neumann, 2009). Microglia cells extend their processes, engulfing particles and retracting them toward their cell body (Kress et al., 2007; Napoli & Neumann, 2009). From what we observed in the current study, the changes in the morphology of microglia may parallel the significant structural rearrangements that are occurring during the same time window, such as dendritic pruning (Paolicelli et al., 2011; Stephan et al., 2012; Whitelaw, 2018), synaptic stripping (Z. Chen et al., 2014; Trapp et al., 2007), synaptogenesis and spine formation/elimination (Miyamoto et al., 2016; Tremblay & Majewska, 2011). From this perspective, microglia may play an essential housekeeping role clearing away excess tissue during the refinement and stabilization of the cortical microcircuit within the barrel cortex.

Impact of Sensory Deprivation on Microglia

Past studies have extensively characterized the effect of chronic sensory deprivation on neuronal morphology (C.-C. Chen, Bajnath, et al., 2015; C.-C. Chen et al., 2012), physiology (Lee, Land, & Simons, 2007; Simons & Land, 1987) and whisker-related behavior (Carvell & Simons, 1990) in the barrel cortex. This study extends these findings by demonstrating that microglia are also impacted by sensory deprivation. We observed microglia exhibiting morphological features consistent with a more activated state, characterized by enlarged cell bodies and retracted processes (Graeber & Streit, 2010). We therefore speculate that, once

activated, microglia assist in the sensory deprivation induced structural rearrangements. Activated microglia are known to secrete proteases, which promote microglia motility, as well as degrade the extracellular matrix (Tremblay & Majewska, 2011). Our current data, along with previous published work (McRae et al., 2007), suggests that microglia may be at least partially responsible for the degradation of extracellular matrix core proteins following sensory deprivation (Chu, Chen, Bajnath, & Brumberg, 2015). The net result allows for the maintenance of a more structurally modifiable environment in the cerebral cortex. Furthermore, microglia have been implicated in synaptic remodeling during development through synaptic stripping (Z. Chen et al., 2014; Trapp et al., 2007; Tremblay et al., 2010) and induction of dendritic spines (Miyamoto et al., 2016). Given the fact that prolonged trimming leads to abnormality of dendritic spines (a proxy of excitatory synapses) in the barrel cortex (C.-C. Chen, Bajnath, et al., 2015), coinciding with our current observation of increased activation of microglia, it is possible that activated microglia play a role in the alterations of synaptic structures within neocortical circuitry during developmentally critical periods (Michell-Robinson et al., 2015; Miyamoto et al., 2016; Rochefort et al., 2002; Tremblay & Majewska, 2011; Ueno & Yamashita, 2014).

It has been previously shown that the activation of $GABA_B$ receptors on microglial cells attenuates their immune response (Kuhn et al., 2004). In addition, several studies have demonstrated that following unilateral whisker clipping, there is a decrease in the density of GABA containing neurons in response to whisker trimming (Micheva & Beaulieu, 1995). Given that microglial cells express $GABA_B$ receptors and their activation attenuates their transition into the activated state (Kuhn et al., 2004) it is possible that the overall deprivation induced decrease of GABA expression in the barrel cortex is responsible for the relatively increased microglial activation that was observed in the chronically deprived animals.

Conclusions

The morphological changes that microglia undergo are indicative of the functional role these cells provide. This dynamic nature allows microglia to adapt in response to different stimuli (Choi et al., 2012; Graeber & Christie, 2012). Under normal development, microglia cells engage in non-pathological roles such as synapses elimination, neuronal apoptosis and axon growth (Arcuri, Mecca, Bianchi, Giambanco, & Donato, 2017b; Dalmau, Vela, González, Finsen, & Castellano, 2003; Hanamsagar et al., 2018; Pont-Lezica et al., 2011; Schafer & Stevens, 2015; Wu et al., 2015). As we have shown in the healthy brain, the morphological phenotype suggests that "inactive" cells populate the CNS, refining and stabilizing the cortical microcircuit within the barrel cortex. The impact of sensory deprivation on microglial activation suggests the cells are engaging in additional non-pathological functions where more "active" cells populate the cortex. We had provided evidence which supports the notion that microglial activation is not an “all or nothing” event, but rather a transition to intermediate states of activation depending on the context of the non-pathological conditions (different developmental age and the sensory experience of the animals), similar to what has been proposed previously (Hanisch & Kettenmann, 2007). The results in the current study, therefore, potentially reflect the need to recruit microglial participation in enabling plasticity during developmentally critical periods and in response to alterations in sensory input.

Acknowledgements

We thank Drs. Carolyn Pytte and Stephan F. Brumberg for helpful comments on the manuscript. Thanks to James Wang for immunocytochemical assistance. The work was supported by a UR/ME grant to JK and SK a CSURP fellowship to RW and PSC-CUNY and NIGMS 1SC3GM122657 grants to JCB.

Availability of data and material

The data that support the findings of this study are available on request from the corresponding author.

Competing interests

The authors declare they have no competing interests

Authors' contributions

Experimental design: JCB, CCC, JK

Data Collection: JK, CCC, SK, TS, RW, CH, CL

Data Analysis JK, CCC, TS

Writing: JK, CCC, JCB

References

Ahmed, Z., Shaw, G., Sharma, V. P., Yang, C., McGowan, E., & Dickson, D. W. (2007). Actin-binding proteins coronin-1a and IBA-1 are effective microglial markers for immunohistochemistry. *The Journal of Histochemistry and Cytochemistry: Official Journal of the Histochemistry Society*, *55*(7), 687–700. https://doi.org/10.1369/jhc.6A7156.2007

Alliot, F., Godin, I., & Pessac, B. (1999). Microglia derive from progenitors, originating from the yolk sac, and which proliferate in the brain. *Brain Research. Developmental Brain Research*, *117*(2), 145–152.

Arcuri, C., Mecca, C., Bianchi, R., Giambanco, I., & Donato, R. (2017a). The Pathophysiological Role of Microglia in Dynamic Surveillance, Phagocytosis and Structural Remodeling of the Developing CNS. *Frontiers in Molecular Neuroscience*, *10*, 191. https://doi.org/10.3389/fnmol.2017.00191

Arcuri, C., Mecca, C., Bianchi, R., Giambanco, I., & Donato, R. (2017b). The Pathophysiological Role of Microglia in Dynamic Surveillance, Phagocytosis and Structural Remodeling of the Developing CNS. *Frontiers in Molecular Neuroscience*, *10*, 191. https://doi.org/10.3389/fnmol.2017.00191

Arnoux, I., Hoshiko, M., Mandavy, L., Avignone, E., Yamamoto, N., & Audinat, E. (2013). Adaptive phenotype of microglial cells during the normal postnatal development of the somatosensory “Barrel” cortex. *Glia*, *61*(10), 1582–1594. https://doi.org/10.1002/glia.22503

Arnoux, I., Hoshiko, M., Sanz Diez, A., & Audinat, E. (2014). Paradoxical effects of minocycline in the developing mouse somatosensory cortex. *Glia*, *62*(3), 399–410. https://doi.org/10.1002/glia.22612

Azevedo, F. A. C., Carvalho, L. R. B., Grinberg, L. T., Farfel, J. M., Ferretti, R. E. L., Leite, R. E. P., … Herculano-Houzel, S. (2009). Equal numbers of neuronal and nonneuronal cells make the human brain an isometrically scaled-up primate brain. *The Journal of Comparative Neurology*, *513*(5), 532–541. https://doi.org/10.1002/cne.21974

Barrera, K., Chu, P., Abramowitz, J., Steger, R., Ramos, R. L., & Brumberg, J. C. (2013). Organization of myelin in the mouse somatosensory barrel cortex and the effects of sensory deprivation. *Developmental Neurobiology*, *73*(4), 297–314. https://doi.org/10.1002/dneu.22060

Carvell, G. E., & Simons, D. J. (1990). Biometric analyses of vibrissal tactile discrimination in the rat. *The Journal of Neuroscience: The Official Journal of the Society for Neuroscience*, *10*(8), 2638–2648.

Carvell, G. E., & Simons, D. J. (1996). Abnormal tactile experience early in life disrupts active touch. *The Journal of Neuroscience: The Official Journal of the Society for Neuroscience*, *16*(8), 2750–2757.

Chen, C.-C., Bajnath, A., & Brumberg, J. C. (2015). The impact of development and sensory deprivation on dendritic protrusions in the mouse barrel cortex. *Cerebral Cortex (New York, N.Y.: 1991)*, *25*(6), 1638–1653. https://doi.org/10.1093/cercor/bht415

Chen, C.-C., Chu, P., & Brumberg, J. C. (2015). Experience-dependent regulation of tissue-type plasminogen activator in the mouse barrel cortex. *Neuroscience Letters*, *599*, 152–157. https://doi.org/10.1016/j.neulet.2015.05.050

Chen, C.-C., Tam, D., & Brumberg, J. C. (2012). Sensory deprivation differentially impacts the dendritic development of pyramidal versus non-pyramidal neurons in layer 6 of mouse barrel cortex. *Brain Structure & Function*, *217*(2), 435–446. https://doi.org/10.1007/s00429-011-0342-9

Chen, Z., Jalabi, W., Hu, W., Park, H.-J., Gale, J. T., Kidd, G. J., … Trapp, B. D. (2014). Microglial displacement of inhibitory synapses provides neuroprotection in the adult brain. *Nature Communications*, *5*, 4486. https://doi.org/10.1038/ncomms5486

Choi, H. K., Ryu, H. J., Kim, J.-E., Jo, S.-M., Choi, H.-C., Song, H.-K., & Kang, T.-C. (2012). The roles of P2X7 receptor in regional-specific microglial responses in the rat brain following status epilepticus. *Neurological Sciences: Official Journal of the Italian Neurological Society and of the Italian Society of Clinical Neurophysiology*, *33*(3), 515–525. https://doi.org/10.1007/s10072-011-0740-z

Chu, P., Chen, E., Bajnath, A., & Brumberg, J. C. (2015). Cell type specificity of tissue plasminogen activator in the mouse barrel cortex. *Data in Brief*, *4*, 332–335. https://doi.org/10.1016/j.dib.2015.06.008

Czeh, M., Gressens, P., & Kaindl, A. M. (2011). The yin and yang of microglia. *Developmental Neuroscience*, *33*(3–4), 199–209. https://doi.org/10.1159/000328989

Dalmau, I., Vela, J. M., González, B., Finsen, B., & Castellano, B. (2003). Dynamics of microglia in the developing rat brain. *The Journal of Comparative Neurology*, *458*(2), 144–157. https://doi.org/10.1002/cne.10572

Erzurumlu, R. S., & Gaspar, P. (2012). Development and critical period plasticity of the barrel cortex. *The European Journal of Neuroscience*, *35*(10), 1540–1553. https://doi.org/10.1111/j.1460-9568.2012.08075.x

Eyo, U. B., & Wu, L.-J. (2013). Bidirectional microglia-neuron communication in the healthy brain. *Neural Plasticity*, *2013*, 456857. https://doi.org/10.1155/2013/456857

Feldman, D. E., & Brecht, M. (2005). Map plasticity in somatosensory cortex. *Science (New York, N.Y.)*, *310*(5749), 810–815. https://doi.org/10.1126/science.1115807

Graeber, M. B., & Christie, M. J. (2012). Multiple mechanisms of microglia: A gatekeeper's contribution to pain states. *Experimental Neurology*, *234*(2), 255–261. https://doi.org/10.1016/j.expneurol.2012.01.007

Graeber, M. B., & Streit, W. J. (2010). Microglia: Biology and pathology. *Acta Neuropathologica*, *119*(1), 89–105. https://doi.org/10.1007/s00401-009-0622-0

Hanamsagar, R., Alter, M. D., Block, C. S., Sullivan, H., Bolton, J. L., & Bilbo, S. D. (2018). Generation of a microglial developmental index in mice and in humans reveals a sex difference in maturation and immune reactivity. *Glia*, *66*(2), 460. https://doi.org/10.1002/glia.23277

Hanisch, U.-K., & Kettenmann, H. (2007). Microglia: Active sensor and versatile effector cells in the normal and pathologic brain. *Nature Neuroscience*, *10*(11), 1387–1394. https://doi.org/10.1038/nn1997

Hart, A. D., Wyttenbach, A., Perry, V. H., & Teeling, J. L. (2012). Age related changes in microglial phenotype vary between CNS regions: Grey versus white matter differences. *Brain, Behavior, and Immunity*, *26*(5), 754–765. https://doi.org/10.1016/j.bbi.2011.11.006

Hoshiko, M., Arnoux, I., Avignone, E., Yamamoto, N., & Audinat, E. (2012). Deficiency of the microglial receptor CX3CR1 impairs postnatal functional development of thalamocortical synapses in the barrel cortex. *The Journal of Neuroscience: The Official Journal of the*

Society for Neuroscience, *32*(43), 15106–15111. https://doi.org/10.1523/JNEUROSCI.1167-12.2012

Italiani, P., & Boraschi, D. (2014). From Monocytes to M1/M2 Macrophages: Phenotypical vs. Functional Differentiation. *Frontiers in Immunology*, *5*, 514. https://doi.org/10.3389/fimmu.2014.00514

Kettenmann, H., Hanisch, U.-K., Noda, M., & Verkhratsky, A. (2011). Physiology of microglia. *Physiological Reviews*, *91*(2), 461–553. https://doi.org/10.1152/physrev.00011.2010

Kigerl, K. A., Gensel, J. C., Ankeny, D. P., Alexander, J. K., Donnelly, D. J., & Popovich, P. G. (2009). Identification of two distinct macrophage subsets with divergent effects causing either neurotoxicity or regeneration in the injured mouse spinal cord. *The Journal of Neuroscience: The Official Journal of the Society for Neuroscience*, *29*(43), 13435–13444. https://doi.org/10.1523/JNEUROSCI.3257-09.2009

Korzhevskii, D. E., & Kirik, O. V. (2016). Brain Microglia and Microglial Markers. *Neuroscience and Behavioral Physiology*, *46*(3), 284–290. https://doi.org/10.1007/s11055-016-0231-z

Kress, H., Stelzer, E. H. K., Holzer, D., Buss, F., Griffiths, G., & Rohrbach, A. (2007). Filopodia act as phagocytic tentacles and pull with discrete steps and a load-dependent velocity. *Proceedings of the National Academy of Sciences of the United States of America*, *104*(28), 11633–11638. https://doi.org/10.1073/pnas.0702449104

Kuhn, S. A., van Landeghem, F. K. H., Zacharias, R., Färber, K., Rappert, A., Pavlovic, S., … Kettenmann, H. (2004). Microglia express GABA(B) receptors to modulate interleukin release. *Molecular and Cellular Neurosciences*, *25*(2), 312–322. https://doi.org/10.1016/j.mcn.2003.10.023

Lawson, L. J., Perry, V. H., Dri, P., & Gordon, S. (1990). Heterogeneity in the distribution and morphology of microglia in the normal adult mouse brain. *Neuroscience*, *39*(1), 151–170. https://doi.org/10.1016/0306-4522(90)90229-w

Lee, S.-H., Land, P. W., & Simons, D. J. (2007). Layer- and cell-type-specific effects of neonatal whisker-trimming in adult rat barrel cortex. *Journal of Neurophysiology*, *97*(6), 4380–4385. https://doi.org/10.1152/jn.01217.2006

McRae, P. A., Rocco, M. M., Kelly, G., Brumberg, J. C., & Matthews, R. T. (2007). Sensory deprivation alters aggrecan and perineuronal net expression in the mouse barrel cortex. *The Journal of Neuroscience: The Official Journal of the Society for Neuroscience*, *27*(20), 5405–5413. https://doi.org/10.1523/JNEUROSCI.5425-06.2007

Michell-Robinson, M. A., Touil, H., Healy, L. M., Owen, D. R., Durafourt, B. A., Bar-Or, A., … Moore, C. S. (2015). Roles of microglia in brain development, tissue maintenance and repair. *Brain: A Journal of Neurology*, *138*(Pt 5), 1138–1159. https://doi.org/10.1093/brain/awv066

Micheva, K. D., & Beaulieu, C. (1995). Neonatal sensory deprivation induces selective changes in the quantitative distribution of GABA-immunoreactive neurons in the rat barrel field cortex. *The Journal of Comparative Neurology*, *361*(4), 574–584. https://doi.org/10.1002/cne.903610403

Miyamoto, A., Wake, H., Ishikawa, A. W., Eto, K., Shibata, K., Murakoshi, H., … Nabekura, J. (2016). Microglia contact induces synapse formation in developing somatosensory cortex. *Nature Communications*, *7*, 12540. https://doi.org/10.1038/ncomms12540

Mosser, C.-A., Baptista, S., Arnoux, I., & Audinat, E. (2017). Microglia in CNS development: Shaping the brain for the future. *Progress in Neurobiology*, *149–150*, 1–20. https://doi.org/10.1016/j.pneurobio.2017.01.002

Napoli, I., & Neumann, H. (2009). Microglial clearance function in health and disease. *Neuroscience*, *158*(3), 1030–1038. https://doi.org/10.1016/j.neuroscience.2008.06.046

Ng, Y. K., & Ling, E. A. (1997). Induction of major histocompatibility class II antigen on microglial cells in postnatal and adult rats following intraperitoneal injections of lipopolysaccharide. *Neuroscience Research*, *28*(2), 111–118.

Nimmerjahn, A., Kirchhoff, F., & Helmchen, F. (2005). Resting microglial cells are highly dynamic surveillants of brain parenchyma in vivo. *Science (New York, N.Y.)*, *308*(5726), 1314–1318. https://doi.org/10.1126/science.1110647

Paolicelli, R. C., Bolasco, G., Pagani, F., Maggi, L., Scianni, M., Panzanelli, P., … Gross, C. T. (2011). Synaptic pruning by microglia is necessary for normal brain development. *Science (New York, N.Y.)*, *333*(6048), 1456–1458. https://doi.org/10.1126/science.1202529

Parkhurst, C. N., & Gan, W.-B. (2010). Microglia dynamics and function in the CNS. *Current Opinion in Neurobiology*, *20*(5), 595–600. https://doi.org/10.1016/j.conb.2010.07.002

Paxinos, G., and Franklin, K. B. J. (2001). *The Mouse Brain in Stereotaxic Coordinates*. San Diego, CA; Academic Press.

Petersen, C. C. H. (2007). The functional organization of the barrel cortex. *Neuron*, *56*(2), 339–355. https://doi.org/10.1016/j.neuron.2007.09.017

Pont-Lezica, L., Béchade, C., Belarif-Cantaut, Y., Pascual, O., & Bessis, A. (2011). Physiological roles of microglia during development. *Journal of Neurochemistry*, *119*(5), 901–908. https://doi.org/10.1111/j.1471-4159.2011.07504.x

Rochefort, N., Quenech'du, N., Watroba, L., Mallat, M., Giaume, C., & Milleret, C. (2002). Microglia and astrocytes may participate in the shaping of visual callosal projections during postnatal development. *Journal of Physiology, Paris*, *96*(3–4), 183–192.

Schafer, D. P., & Stevens, B. (2015). Microglia Function in Central Nervous System Development and Plasticity. *Cold Spring Harbor Perspectives in Biology*, *7*(10), a020545. https://doi.org/10.1101/cshperspect.a020545

Shapiro, L. A., Perez, Z. D., Foresti, M. L., Arisi, G. M., & Ribak, C. E. (2009). Morphological and ultrastructural features of Iba1-immunolabeled microglial cells in the hippocampal dentate gyrus. *Brain Research*, *1266*, 29–36. https://doi.org/10.1016/j.brainres.2009.02.031

Sholl, D. A. (1956). The measurable parameters of the cerebral cortex and their significance in its organization. *Progress in Neurobiology*, (2), 324–333.

Simons, D. J., & Land, P. W. (1987). Early experience of tactile stimulation influences organization of somatic sensory cortex. *Nature*, *326*(6114), 694–697. https://doi.org/10.1038/326694a0

Stephan, A. H., Barres, B. A., & Stevens, B. (2012). The complement system: An unexpected role in synaptic pruning during development and disease. *Annual Review of Neuroscience*, *35*, 369–389. https://doi.org/10.1146/annurev-neuro-061010-113810

Stevens, B., Allen, N. J., Vazquez, L. E., Howell, G. R., Christopherson, K. S., Nouri, N., … Barres, B. A. (2007). The classical complement cascade mediates CNS synapse elimination. *Cell*, *131*(6), 1164–1178. https://doi.org/10.1016/j.cell.2007.10.036

The Mouse Brain in Stereotaxic Coordinates, Compactâ”3rd Edition. (n.d.). Retrieved August 16, 2019, from https://www.elsevier.com/books/the-mouse-brain-in-stereotaxic-coordinates-compact/franklin/978-0-12-374244-5

Trapp, B. D., Wujek, J. R., Criste, G. A., Jalabi, W., Yin, X., Kidd, G. J., … Ransohoff, R. (2007). Evidence for synaptic stripping by cortical microglia. *Glia*, *55*(4), 360–368. https://doi.org/10.1002/glia.20462

Tremblay, M.-È., Lowery, R. L., & Majewska, A. K. (2010). Microglial interactions with synapses are modulated by visual experience. *PLoS Biology*, *8*(11), e1000527. https://doi.org/10.1371/journal.pbio.1000527

Tremblay, M.-È., & Majewska, A. K. (2011). A role for microglia in synaptic plasticity? *Communicative & Integrative Biology*, *4*(2), 220–222. https://doi.org/10.4161/cib.4.2.14506

Ueno, M., Fujita, Y., Tanaka, T., Nakamura, Y., Kikuta, J., Ishii, M., & Yamashita, T. (2013). Layer V cortical neurons require microglial support for survival during postnatal development. *Nature Neuroscience*, *16*(5), 543–551. https://doi.org/10.1038/nn.3358

Ueno, M., & Yamashita, T. (2014). Bidirectional tuning of microglia in the developing brain: From neurogenesis to neural circuit formation. *Current Opinion in Neurobiology*, *27*, 8–15. https://doi.org/10.1016/j.conb.2014.02.004

Villa, P., van Beek, J., Larsen, A. K., Gerwien, J., Christensen, S., Cerami, A., … Torup, L. (2007). Reduced functional deficits, neuroinflammation, and secondary tissue damage

after treatment of stroke by nonerythropoietic erythropoietin derivatives. *Journal of Cerebral Blood Flow and Metabolism: Official Journal of the International Society of Cerebral Blood Flow and Metabolism*, *27*(3), 552–563. https://doi.org/10.1038/sj.jcbfm.9600370

Vinet, J., Vainchtein, I. D., Spano, C., Giordano, C., Bordini, D., Curia, G., … Biagini, G. (2016). Microglia are less pro-inflammatory than myeloid infiltrates in the hippocampus of mice exposed to status epilepticus. *Glia*, *64*(8), 1350–1362. https://doi.org/10.1002/glia.23008

Whitelaw, B. S. (2018). Microglia-mediated synaptic elimination in neuronal development and disease. *Journal of Neurophysiology*, *119*(1), 1–4. https://doi.org/10.1152/jn.00021.2017

Wu, Y., Dissing-Olesen, L., MacVicar, B. A., & Stevens, B. (2015). Microglia: Dynamic Mediators of Synapse Development and Plasticity. *Trends in Immunology*, *36*(10), 605–613. https://doi.org/10.1016/j.it.2015.08.008

.

Figure Legends

Figure 1. Microglial morphology. Coronal sections through barrel cortex of P2(A),P7 (B), P14 (C), P45 (E), P60 (F) under high magnification labeled with the antibody to Iba-1. Our staining produced high resolution of morphological features of the somata and processes. Scale bar = 10μm for all panels.

Figure 2. Microglial reconstructions. Representative reconstructed microglial cells within layer IV of the barrel cortex. Reconstructed microglial cells from the control group at different developmental ages; P2 (A), P14 (B), P30 (C), P45 (D), and P60 (E). All scale bars 10 μm.

Figure 3. Iba-1 **expression varies across laminae and development.** A: Coronal view of Iba-1 stained barrel cortex with contours indicating layers 2/3, 4, 5, 6 and the cortical white matter. The brightness of the individual layers was divided by the area of the contour map generated and were normalized to the brightness and area of the white matter of that specific animal (Optical density = [brightness of cortical layer]/[brightness of white matter]). Scale bar = 250 μm. B: Optical density measurements on overall expression patterns of Iba-1 as a function of age. Data are from control animals, means and one standard error of the mean are represented. Laminae were determined by cellular density and size determined by Hoechst staining (not shown).

Figure 4. Quantification of morphological features. Morphological measurements of reconstructed microglial cells in layer IV of barrel cortex as a function of age. Morphological measurements include, A: cell body area, B: cell body perimeter C: somatic aspect ratio, D: number of processes, E: processes ends, F: process length. Data represent population means,

error bars indicate one standard error of the mean (SEM). Asterisks indicates statistical significance for all pair-wise comparisons following rank-based ANOVA ($p<0.05$).

Figure 5. Sholl analyses. The starting radius was at 10 μm from the cell perimeter with a radius increment of 5 μm. Using concentric sphere analysis, we focused on the process length and number of intersections. A: Process Length as a function of distance away from the soma. B. Number of intersections as a function of distance away from the soma. Data represent population means, Error bars indicate one standard error of the mean (SEM).

Figure 6. Sensory deprivation does not impact overall expression of Iba-1. (A) Optical density measurements of Iba-1 expression as a function of cortical lamina in control (open bars) and trimmed (solid bars) conditions. (B) Stereological quantification method of Iba-1 expression as a function of cortical lamina in control (open bars) and trimmed (solid bars) conditions, the stereological analysis results in an unbiased estimate of microglia population (see methods). The difference between control and trimmed condition for both experiments was not statistically significant between any pair. Bars represent population means and error bars represent SEM.

Figure 7 Sensory deprivation's impact on microglia morphology. A Iba-1+ microglia from a P30 animal (A) has a small cell body with spindly processes. In contrast, following 30 days of whisker trimming the cell body enlarges and the processes retract (B). Following 30 days of whisker regrowth P60 microglia are indistinguishable (C, D). See Figure 8 for quantification.

Figure 8. Sensory deprivation impacts microglial morphology. Comparison between reconstructed barrel cortex layer IV microglial cells in the P30 nondeprived cortex (P30 control, A) and sensory deprived barrel cortex animals (P30 trim, B) showed increased cell body size and retraction of processes following trimming. Following sensory restoration the control (C) and regrow group (D) did not differ from each other. All scale bars show 10 μm. Sensory deprivation did not alter the number of processes across all groups. (E), but a statistical decrease in the process length (F) was observed as well as an increase in the number of processes ends between treatment groups and respective controls (G). Concomitantly with these changes, a statistical increase was observed in the size of the cell body (μm) in the sensory deprived microglia (P30 trim) compared with control P30 cortices (H). For the box and whisker plots the solid black lines represent population medians, whereas the dotted white lines represent population means. Error bars indicate standard error of the mean (SEM). Asterisks indicates statistical significance for all pair-wise comparisons following rank-based ANOVA ($p<0.05$).

Figure 9. Microglia surface receptor expression following sensory deprivation: Sample confocal images from a sensory deprived (Row A) and a control (Row B) animal. Number of total cells in a z-stack was determined from Hoechst staining (blue, A_1, B_1). All microglia were labeled with Iba-1 (magenta, A_2, B_2), and a smaller proportion were also immunoreactive for MHC-II (green, A_3, B_3). The images show ramified microglia with small somas and many branched processes. The overlay of all the channels shows colocalization between Iba-1+ and MHC-II+ cells (indicated with asterisks) (A_4, B_4) and Iba-1+ microglia that do not express MHC-II are indicated with arrows. Scale bar (25 μm) is the same for all panels. Neither the overall microglia density (as measured by Iba-1+ cells) nor activated microglia density (as

measured by MHC-II+ cells) change significantly following one month of sensory deprivation (C). The relative proportion of MHC-II+ microglia did not change as a result of sensory deprivation (D). Bar charts plot population means and one SEM.

Supplemental Table Legends

Supplemental Table 1. Microglia densities are highest in the supragranular layers. A composite analysis [Repeated Measures ANOVA (Tukey HSD test)] as a function of cortical lamina in the barrel cortex across development time (P2: n=6 animals, P14: n= 5 animals, P30: n= 7 animals, P45: n= 3 animals, P60: n= 3 animals) revealed that microglia density is statistically higher in layer 2/3 of the barrel cortex. Values represent statistical significance for all pair-wise comparisons following rank-based ANOVA ($p<0.05$).

Supplemental Table 2. Microglia density varies as a function of developmental age. Mixed-Model ANOVA (Post-hoc: Tukey test) as a function of cortical lamina in the barrel cortex across development (P2: n=3 animals, P14: n= 5 animals, P30: n= 7 animals, P45: n= 3 animals, P60: n= 3 animals) revealed that microglia numbers increased up to P45, independent of which lamina was observed. Microglia numbers returned to baseline levels following about two months of age (P60). Values represent statistical significance for all pair-wise comparisons following rank-based ANOVA ($p<0.05$).

Supplemental Table 3. Number of intersections increases as a function of distance away from the microglial soma until P30. Sholl analysis, mixed-model ANOVA (condition × distance from soma) was performed for the number of intersections. Subsequently, Scheffé's method was used as a post hoc protocol for comparisons between conditions (P2: n=3 animals, P14: n= 4 animals, P30: n= 7 animals, P45: n= 5 animals, P60: n= 3 animals). The starting radius was at 10μm with a radius increment of 5μm. The results revealed a steady increase ($p<0.04$) in the number of intersections (10-15 μm) up until P30, dropping back down by P60. Values

represent statistical significance for all pair-wise comparisons following rank-based ANOVA ($p<0.04$).

Supplemental Table 4. A steady increase in length of the processes is observed up to P30, as a function of distance away from the microglial soma. Sholl analysis, mixed-model ANOVA (condition × distance from soma) was performed for the number of intersections. Subsequently, Scheffé's method was used as a post hoc protocol for comparisons between conditions (P2: n=3 animals, P14: n= 4 animals, P30: n= 7 animals, P45: n= 5 animals, P60: n= 3 animals). The starting radius was at 10μm with subsequent radius increments of 5μm. The results revealed a steady increase ($p<0.04$) in the length of the processes up until P30, dropping back down by P60. Values represent statistical significance for all pair-wise comparisons following rank-based ANOVA ($p<0.04$).

Table 1. Experimental Groups. The number of animals and cells reconstructed from each group. In some cases groups are used for multiple comparisons as indicated in the text. For optical density and stereology studies n=number of animals. P30 Control brains are from the hemisphere ipsilateral to the trimming whereas the P30 Trim sections are derived from the same animals using the barrel cortex contralateral to the trimming.

Group	**Animals**	**Microglia Reconstructed**
P2 Control	6	20
P14 Control	9	20
P30 Control	7	20
P45 Control	8	20
P60 Control	6	20
P30 Trim	7	16
P60 Regrow	4	17

Table 2. Sensory deprivation impacts microglial cell bodies. Pairwise comparisons (student t-test) between control (P30 Control, n=7 animals, 16 cells) and trim animals (P30 Trim, n=7 animals, 15 cells) revealed that following one month of sensory deprivation the cell body uniformly expanded without impacting its shape. Values represent population means, standard deviation and p values.

	P30 Control		P30 Trim		
	Mean	**SD**	**Mean**	**SD**	**P-value**
Perimeter (μm)*	**28.16**	**6.63**	**31.19**	**6.94**	**0.004**
Area (μm²)*	**40.56**	**20.55**	**49.31**	**22.54**	**0.008**
Feret Max (μm)*	**10.45**	**2.51**	**11.39**	**2.79**	**0.019**
Feret Min (μm)*	**5.74**	**1.90**	**6.54**	**1.66**	**0.004**
Aspect Ratio*	**1.95**	**0.64**	**1.79**	**0.44**	**0.041**
Compactness	0.68	0.11	0.69	0.09	0.191
Convexity	0.94	0.04	0.93	0.03	0.170
Form Factor	0.62	0.13	0.62	0.12	0.396
Roundness	0.47	0.15	0.48	0.12	0.237
Solidity	0.89	0.06	0.88	0.06	0.272

Graphical Abstract Legend

Mice were either reared with intact whiskers or unilaterally trimmed for the first post-natal month. Subsequent evaluation of Microglia within their barrel cortex revealed that peripheral whisker trimming results in enlarged microglia somata and retraction of their processes. These results suggest that peripheral sensory input can shape microglial responses within the mouse barrel cortex. Scale bar represents 10 μm.

	Layer 2/3	Layer 4	Layer 4	Layer 6	White Matter
Layer 2/3		0.000137	0.000133	0.000133	0.000133
Layer 4	0.000137		0.048746	N/S	0.005103
Layer 4	0.000133	0.048746		N/S	N/S
Layer 6	0.000133	N/S	N/S		N/S
White Matter	0.000133	0.005103	N/S	N/S	

Tukey HSD test; variable DV (optical density)
Approximate Probabilities for Post Hoc Tests
Error: Within MS = .00215, df = 60.000

Table S2A
layer 2/3

	P7	P14	P30	P45	P60
P7		0.926354	0.994402	0.184737	0.410895
P14	0.926354		0.989904	0.022643	0.710557
P30	0.994402	0.989904		0.057260	0.511293
P45	0.184737	0.022643	0.057260		0.006708
P60	0.410895	0.710557	0.511293	0.006708	

TUKEY test; variable **later 2/3** (optical density)
Probabilities for Post Hoc Tests
Error: Between MS = .00938, df = 15.000

Table S2B
layer 4

	P7	P14	P30	P45	P60
P7		0.948643	0.996883	0.702531	0.378303
P14	0.948643		0.992002	0.229858	0.620436
P30	0.996883	0.992002		0.420695	0.440368
P45	0.702531	0.229858	0.420695		0.044831
P60	0.378303	0.620436	0.440368	0.044831	

TUKEY test; variable **layer 4** (optical density)
Probabilities for Post Hoc Tests
Error: Between MS = .00734, df = 15.000

Table S2C
layer 5

	P7	P14	P30	P45	P60
P7		0.996094	0.999836	0.251269	0.734007
P14	0.996094		0.970549	0.078940	0.822030
P30	0.999836	0.970549		0.218254	0.554817
P45	0.251269	0.078940	0.218254		0.028918
P60	0.734007	0.822030	0.554817	0.028918	

TUKEY test; variable **layer** 5 (optical density)
Probabilities for Post Hoc Tests
Error: Between MS = .00406, df = 15.000

Table S2D
layer 6

TUKEY test; variable **layer 6** (optical density)
Probabilities for Post Hoc Tests
Error: Between MS = .00215, df = 15.0

	P7	P14	P30	P45	P60
P7		0.972075	0.932193	0.012863	0.998184
P14	0.972075		0.999288	0.013298	0.873894
P30	0.932193	0.999288		0.024357	0.797802
P45	0.012863	0.013298	0.024357		0.007275
P60	0.998184	0.873894	0.797802	0.007275	

Table S2E
White Matter

	P7	P14	P30	P45	P60
P7		0.400947	0.643489	0.616902	0.839577
P14	0.400947		0.991081	0.999845	0.967705
P30	0.643489	0.991081		0.999506	0.999207
P45	0.616902	0.999845	0.999506		0.993620
P60	0.839577	0.967705	0.999207	0.993620	

Tukey test; variable white matter (optical density)
Probabilities for Post Hoc Tests
Error: Between MS = .00004, df = 15.000

Table S3A
Sholl Intersections/Layer 4
10.00

	P60 control	P45 control	P30 control	P14 control	P2 control
P60 control		0.680510	0.213939	0.400728	0.760888
P45 control	0.680510		0.894619	0.980223	0.124978
P30 control	0.213939	0.894619		0.998185	**0.021345**
P14 control	0.400728	0.980223	0.998185		0.055661
P2 control	0.760888	0.124978	**0.021345**	0.055661	

Scheffe test; variable 10.000000 (updated sholl intersections)
Probabilities for Post Hoc Tests
Error: Between MS = 11.236, df = 52.000

Table S3B
15.00

	P60 control	P45 control	P30 control	P14 control	P2 control
P60 control		0.796183	0.338005	0.767860	0.755817
P45 control	0.796183		0.920291	0.999890	0.179164
P30 control	0.338005	0.920291		0.970602	**0.039986**
P14 control	0.767860	0.999890	0.970602		0.187213
P2 control	0.755817	0.179164	**0.039986**	0.187213	

Scheffe test; variable 15.000000 (updated sholl intersections)
Probabilities for Post Hoc Tests
Error: Between MS = 11.747, df = 52.000

Table S3C
20.00

	P60 control	P45 control	P30 control	P14 control	P2 control
P60 control		0.348871	**0.002667**	0.428667	0.995902
P45 control	0.348871		0.250135	1.000000	0.696922
P30 control	**0.002667**	0.250135		0.339438	**0.022662**
P14 control	0.428667	1.000000	0.339438		0.740755
P2 control	0.995902	0.696922	**0.022662**	0.740755	

Scheffe test; variable 20.000000 (updated sholl intersections)
Probabilities for Post Hoc Tests
Error: Between MS = 9.4990, df = 52.000

Table S3D
25.00

	P60 control	P45 control	P30 control	P14 control	P2 control
P60 control		0.722010	**0.002047**	0.939929	0.989322
P45 control	0.722010		0.059761	0.995326	0.967810
P30 control	**0.002047**	0.059761		**0.040057**	**0.024657**
P14 control	0.939929	0.995326	**0.040057**		0.999118
P2 control	0.989322	0.967810	**0.024657**	0.999118	

Scheffe test; variable 25.000000 (updated sholl intersections)
Probabilities for Post Hoc Tests
Error: Between MS = 5.0945, df = 52.000

Table S3E
30.00

	P60 control	P45 control	P30 control	P14 control	P2 control
P60 control		0.967523	**0.019695**	0.656285	0.453278
P45 control	0.967523		0.087066	0.936377	0.796690
P30 control	**0.019695**	0.087066		0.493164	0.739738
P14 control	0.656285	0.936377	0.493164		0.997167
P2 control	0.453278	0.796690	0.739738	0.997167	

Scheffe test; variable 30.000000 (updated sholl intersections)
Probabilities for Post Hoc Tests
Error: Between MS = 2.6044, df = 52.000

Table S3F
35.00

	P60 control	P45 control	P30 control	P14 control	P2 control
P60 control		0.999813	0.057922	0.999917	0.359073
P45 control	0.999813		0.077348	0.998257	0.432883
P30 control	0.057922	0.077348		0.063419	0.955200
P14 control	0.999917	0.998257	0.063419		0.345897
P2 control	0.359073	0.432883	0.955200	0.345897	

Scheffe test; variable 35.000000 (updated sholl intersections)
Probabilities for Post Hoc Tests
Error: Between MS = .64374, df = 52.000

Table S3G
40.00

	P60 control	P45 control	P30 control	P14 control	P2 control
P60 control		0.968779	0.496634	0.999521	0.957338
P45 control	0.968779		0.844499	0.926929	0.999933
P30 control	0.496634	0.844499		0.430026	0.932513
P14 control	0.999521	0.926929	0.430026		0.913481
P2 control	0.957338	0.999933	0.932513	0.913481	

Scheffe test; variable 40.000000 (updated sholl intersections)
Probabilities for Post Hoc Tests
Error: Between MS = .54472, df = 52.000

Table S3H
45.00

	P60 control	P45 control	P30 control	P14 control	P2 control
P60 control		0.860328	0.976237	1.000000	0.959967
P45 control	0.860328		0.996982	0.889129	0.999654
P30 control	0.976237	0.996982		0.981270	0.999953
P14 control	1.000000	0.889129	0.981270		0.967487
P2 control	0.959967	0.999654	0.999953	0.967487	

Scheffe test; variable 45.000000 (updated sholl intersections)
Probabilities for Post Hoc Tests
Error: Between MS = .10601, df = 52.000

Table S3I
50.00

	P60 control	P45 control	P30 control	P14 control	P2 control
P60 control		0.783247	0.991016	1.000000	1.000000
P45 control	0.783247		0.970157	0.824869	0.840832
P30 control	0.991016	0.970157		0.992975	0.993696
P14 control	1.000000	0.824869	0.992975		1.000000
P2 control	1.000000	0.840832	0.993696	1.000000	

Scheffe test; variable 50.000000 (updated sholl intersections)
Probabilities for Post Hoc Tests
Error: Between MS = .17820, df = 52.000

Table S3J
55.00

	P60 control	P45 control	P30 control	P14 control	P2 control
P60 control		0.912436	0.843987	1.000000	1.000000
P45 control	0.912436		0.999445	0.931439	0.938464
P30 control	0.843987	0.999445		0.872506	0.883555
P14 control	1.000000	0.931439	0.872506		1.000000
P2 control	1.000000	0.938464	0.883555	1.000000	

Scheffe test; variable 55.000000 (updated sholl intersections)
Probabilities for Post Hoc Tests
Error: Between MS = .14136, df = 52.000

Table S3K
60.00

	P60 control	P45 control	P30 control	P14 control	P2 control
P60 control		0.749178	1.000000	1.000000	1.000000
P45 control	0.749178		0.779107	0.795855	0.813918
P30 control	1.000000	0.779107		1.000000	1.000000
P14 control	1.000000	0.795855	1.000000		1.000000
P2 control	1.000000	0.813918	1.000000	1.000000	

Scheffe test; variable 60.000000 (updated sholl intersections)
Probabilities for Post Hoc Tests
Error: Between MS = .07143, df = 52.000

Table S3L
65.00

	P60 control	P45 control	P30 control	P14 control	P2 control
P60 control		0.749178	1.000000	1.000000	1.000000
P45 control	0.749178		0.779107	0.795855	0.813918
P30 control	1.000000	0.779107		1.000000	1.000000
P14 control	1.000000	0.795855	1.000000		1.000000
P2 control	1.000000	0.813918	1.000000	1.000000	

Scheffe test; variable 65.000000 (updated sholl intersections)
Probabilities for Post Hoc Tests
Error: Between MS = .28571, df = 52.000

Table S4A
Sholl Length/Layer 4
10.00

	P60 control	P45 control	P30 control	P14 control	P2 control
P60 control		0.624239	0.991864	0.895033	0.337126
P45 control	0.624239		0.899099	0.995046	**0.016634**
P30 control	0.991864	0.899099		0.991192	0.182020
P14 control	0.895033	0.995046	0.991192		0.077666
P2 control	0.337126	**0.016634**	0.182020	0.077666	

Scheffe test; variable 10.000000 (updated sholl length)
Probabilities for Post Hoc Tests
Error: Between MS = 557.56, df = 52.000

Table S4B
15.00

	P60 control	P45 control	P30 control	P14 control	P2 control
P60 control		0.974994	0.643086	0.462489	0.284260
P45 control	0.974994		0.921814	0.791590	0.087682
P30 control	0.643086	0.921814		0.998082	**0.017064**
P14 control	0.462489	0.791590	0.998082		**0.008755**
P2 control	0.284260	0.087682	**0.017064**	**0.008755**	

Scheffe test; variable 15.000000 (updated sholl length)
Probabilities for Post Hoc Tests
Error: Between MS = 700.70, df = 52.000

Table S4C
20.00

	P60 control	P45 control	P30 control	P14 control	P2 control
P60 control		0.885103	**0.035013**	0.611611	0.906294
P45 control	0.885103		0.241456	0.977208	0.422438
P30 control	**0.035013**	0.241456		0.660244	**0.006242**
P14 control	0.611611	0.977208	0.660244		0.213560
P2 control	0.906294	0.422438	**0.006242**	0.213560	

Scheffe test; variable 20.000000 (updated sholl length)
Probabilities for Post Hoc Tests
Error: Between MS = 498.81, df = 52.000

Table S4D
25.00

	P60 control	P45 control	P30 control	P14 control	P2 control
P60 control		0.532489	**0.002649**	0.506481	0.999992
P45 control	0.532489		0.140198	0.999794	0.680345
P30 control	**0.002649**	0.140198		0.276475	**0.009730**
P14 control	0.506481	0.999794	0.276475		0.639865
P2 control	0.999992	0.680345	**0.009730**	0.639865	

Scheffe test; variable 25.000000 (updated sholl length)
Probabilities for Post Hoc Tests
Error: Between MS = 315.69, df = 52.000

Table S4E
30.00

	P60 control	P45 control	P30 control	P14 control	P2 control
P60 control		0.812644	**0.008458**	0.991988	0.986212
P45 control	0.812644		0.119302	0.980247	0.990537
P30 control	**0.008458**	0.119302		0.051967	0.076663
P14 control	0.991988	0.980247	0.051967		0.999992
P2 control	0.986212	0.990537	0.076663	0.999992	

Scheffe test; variable 30.000000 (updated sholl length)
Probabilities for Post Hoc Tests
Error: Between MS = 167.96, df = 52.000

Table S4F
35.00

	P60 control	P45 control	P30 control	P14 control	P2 control
P60 control		0.895687	0.053409	0.999834	0.693658
P45 control	0.895687		0.307389	0.962163	0.987007
P30 control	0.053409	0.307389		0.118025	0.721592
P14 control	0.999834	0.962163	0.118025		0.820131
P2 control	0.693658	0.987007	0.721592	0.820131	

Scheffe test; variable 35.000000 (updated sholl length)
Probabilities for Post Hoc Tests
Error: Between MS = 90.758, df = 52.000

Table S4G
40.00

	P60 control	P45 control	P30 control	P14 control	P2 control
P60 control		0.999290	0.203975	0.999992	0.788530
P45 control	0.999290		0.289742	0.998253	0.882324
P30 control	0.203975	0.289742		0.229141	0.907634
P14 control	0.999992	0.998253	0.229141		0.785137
P2 control	0.788530	0.882324	0.907634	0.785137	

Scheffe test; variable 40.000000 (updated sholl length)
Probabilities for Post Hoc Tests
Error: Between MS = 31.841, df = 52.000

Table S4H
45.00

	P60 control	P45 control	P30 control	P14 control	P2 control
P60 control		0.860568	0.683811	1.000000	0.871779
P45 control	0.860568		0.995040	0.873755	0.999988
P30 control	0.683811	0.995040		0.711735	0.998849
P14 control	1.000000	0.873755	0.711735		0.879917
P2 control	0.871779	0.999988	0.998849	0.879917	

Scheffe test; variable 45.000000 (updated sholl length)
Probabilities for Post Hoc Tests
Error: Between MS = 11.300, df = 52.000

Table S4I
50.00

	P60 control	P45 control	P30 control	P14 control	P2 control
P60 control		0.863765	0.920379	1.000000	0.999800
P45 control	0.863765		0.999984	0.891949	0.954241
P30 control	0.920379	0.999984		0.936090	0.976141
P14 control	1.000000	0.891949	0.936090		0.999841
P2 control	0.999800	0.954241	0.976141	0.999841	

Scheffe test; variable 50.000000 (updated sholl length)
Probabilities for Post Hoc Tests
Error: Between MS = 7.3302, df = 52.000

Table S4J
55.00

	P60 control	P45 control	P30 control	P14 control	P2 control
P60 control		0.884417	0.887777	1.000000	1.000000
P45 control	0.884417		0.999999	0.908807	0.917902
P30 control	0.887777	0.999999		0.909184	0.917383
P14 control	1.000000	0.908807	0.909184		1.000000
P2 control	1.000000	0.917902	0.917383	1.000000	

Scheffe test; variable 55.000000 (updated sholl length)
Probabilities for Post Hoc Tests
Error: Between MS = 4.8900, df = 52.000

Table S4K
60.00

	P60 control	P45 control	P30 control	P14 control	P2 control
P60 control		0.868317	0.910151	1.000000	1.000000
P45 control	0.868317		0.999999	0.895677	0.905928
P30 control	0.910151	0.999999		0.927687	0.934362
P14 control	1.000000	0.895677	0.927687		1.000000
P2 control	1.000000	0.905928	0.934362	1.000000	

Scheffe test; variable 60.000000 (updated sholl length)
Probabilities for Post Hoc Tests
Error: Between MS = 5.7044, df = 52.000

Table S4L
65.00

	P60 control	P45 control	P30 control	P14 control	P2 control
P60 control		0.749178	1.000000	1.000000	1.000000
P45 control	0.749178		0.779107	0.795855	0.813918
P30 control	1.000000	0.779107		1.000000	1.000000
P14 control	1.000000	0.795855	1.000000		1.000000
P2 control	1.000000	0.813918	1.000000	1.000000	

Scheffe test; variable 65.000000 (updated sholl length)
Probabilities for Post Hoc Tests
Error: Between MS = 2.8350, df = 52.000

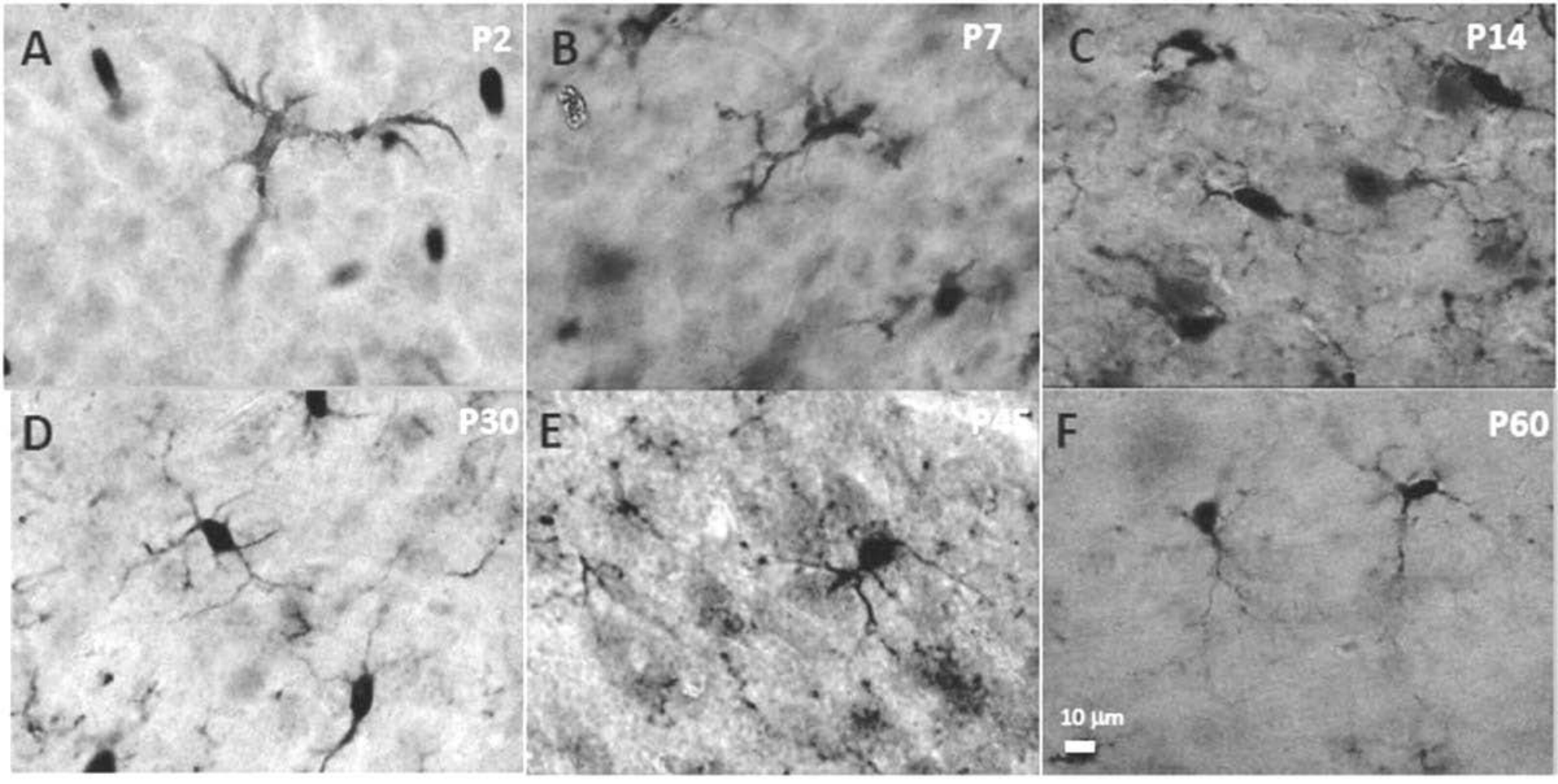
A
P2
B
P7
C
P14
D
P30
E
F
P60
10 µm